Journal of Power Sources 234 (2013) 111–118

Contents lists available at SciVerse ScienceDirect

Journal of Power Sources

journal homepage: www.elsevier.com/locate/jpowsour

Quantitative estimation of water vapor distribution in low-humidity proton exchange membrane fuel cell using humidity test paper

Kosuke Nishida [a,*], Yoma Yokoi [a], Masaya Asa [a], Shohji Tsushima [b], Shuichiro Hirai [b]

[a] Department of Mechanical and System Engineering, Kyoto Institute of Technology, Matsugasaki, Sakyo-ku, Kyoto 606-8585, Japan
[b] Department of Mechanical and Control Engineering, Tokyo Institute of Technology, 2-12-1 Ohokayama, Meguro-ku, Tokyo 152-8552, Japan

HIGHLIGHTS

- In low-humidity PEMFCs, fundamental understanding of water transport on anode side is required.
- This paper presents a method for measuring water vapor distribution using humidity test paper.
- Effects of humidification and flow configuration on water and current profiles are investigated.
- High humidification of anode inlet enhances water concentration in anode and prevents dryout.
- Counter-flow configuration improves water management and proton conductivity at anode inlet.

ARTICLE INFO

Article history:
Received 18 September 2012
Received in revised form
5 January 2013
Accepted 28 January 2013
Available online 8 February 2013

Keywords:
Proton exchange membrane fuel cell
Low-humidity operation
Water transport
Dryout
Humidity test paper

ABSTRACT

To prevent performance degradation due to membrane dryout in proton exchange membrane fuel cells (PEMFCs) under low-humidity conditions, fundamental understanding of water transport and reaction mechanism on anode side in operating fuel cell is required. In this study, the water vapor distribution along the anode flow channel of a low-humidity PEMFC was quantitatively evaluated by using humidity test paper (HTP), and the effects of inlet gas humidification and flow configuration on the water distribution in the anode were investigated. HTP is a test paper for detecting water vapor in the range of 20–90% RH, and makes it possible to directly visualize the water distribution in the gas flow channel of the transparent PEMFC during operation. Furthermore, the locally resolved current density was also measured using segmented cell structure concept. It was found that the high humidification of the anode inlet gas increases the water vapor concentration in the anode channel and prevents the membrane dehydration. In addition, the counter-flow configuration effectively improves the water management near the anode inlet region of the low-humidity PEMFC and enhances the proton conductivity in the electrolyte membrane.

1. Introduction

Low-humidity operation of proton exchange membrane fuel cells (PEMFCs) is preferred especially in automotive applications because of their compact design. However, water management in anode of low-humidity PEMFC is essential for maintaining sufficient membrane hydration and high proton conductivity. During the operation of a PEMFC at high current densities, water migrates significantly through the electrolyte membrane from the anode to cathode owing to electro-osmotic drag. Thus, the membrane dehydration occurs mainly on the anode side under low-humidity conditions. In order to alleviate this issue known as “dryout”, it is essential to understand the fundamental phenomena of the water transport and electrode reaction at the anode side in an operating PEMFC.

Many researchers have conducted visualization studies to probe water transport in working PEMFCs [1–19]. Liquid water formation, accumulation and removal inside PEMFCs were investigated by neutron radiography [1–8], soft X-ray radiography [9], X-ray computed tomography [10,11], and optical visualization using transparent fuel cells [12–17]. Water content distribution in proton exchange membrane (PEM) was observed by using magnetic resonance imaging (MRI) [18]. In addition, water vapor distribution within cathode gas diffusion layer (GDL) was detected with the use of water sensitive paper (WSP) [19]. However, the WSP measurement technique is a qualitative methodology, and cannot quantitatively

* Corresponding author. Tel./fax: +81 75 724 7321.
E-mail address: knishida@kit.ac.jp (K. Nishida).

0378-7753/$ – see front matter © 2013 Elsevier B.V. All rights reserved.
http://dx.doi.org/10.1016/j.jpowsour.2013.01.160

estimate water vapor distribution. Several authors have made experimental efforts to measure water vapor and current distributions in PEMFCs under low-humidity operation using gas chromatograph (GC) and segmented cell structure [20–25]. It has been reported that the water vapor profile along the anode channel of a low-humidity PEMFC is closely tied to the water transport through the membrane due to the back-diffusion and electro-osmotic drag. In the case of dry anode inlet, the water vapor concentration increases monotonically along the anode flow path owing to the strong back-diffusion of water from the cathode to anode [22,24]. In contrast, if the cathode inlet is drier than the anode inlet, the anode water distribution first decreases to the minimum point along the flow channel due to the electro-osmotic drag and forward-diffusion from the anode to cathode. After the minimum point, the water concentration then increases due to the back-diffusion of water. Dong et al. [22] demonstrated that the anode water profile contributes significantly to the overall performance of a fuel cell operated at low-humidity conditions. The cell performance is highly coupled to the water vapor content in the anode inlet region, because the electro-osmotic drag acts to dry the anode side and is not completely compensated by the back-diffusion. Liu et al. [24] revealed that minimum current densities are observed at the fuel cell inlet, and increase monotonically toward the outlet as the electrolyte membrane takes up water. To elucidate water transport through electrolyte membrane, Lu et al. [25] first developed a method to determine the distribution of net water crossover coefficient along the flow direction by simultaneously measuring the water concentration and current density distributions. Although many experimental studies have been examined as mentioned above, water transport and reaction distribution on anode side during low-humidity PEMFC operation are not fully understood because of their complexity. Water and current distributions in operating fuel cell depend on many parameters including overall current, cell temperature, gas stoichiometries, inlet humidification, electrolyte thickness and flow-field design. In the previous studies, most researchers have investigated water and current distributions only in the co-flow cell [20–25], and have not compared water behaviors in both co-flow and counter-flow cases.

This paper first presents a novel method for quantitatively measuring the water vapor distribution in the anode channel of an operating PEMFC using humidity test paper (HTP). HTP is a test paper for detecting water vapor of 20–90% RH. This test paper is inserted between the anode GDL and separator in the transparent cell, and enables to visualize the water distribution in the anode flow field during low-humidity operation. The discoloration image of HTP can be quantitatively converted to water vapor concentration based on the image processing. Although quantitative evaluation of water vapor distribution in PEMFCs has been conventionally carried out by using micro GC [20–25] and tunable diode laser absorption spectroscopy (TDLAS) [26], these equipments are special and expensive. The measurement technique proposed in this study can provide the same information without the use of specialized equipment. Furthermore, we have reported a somewhat similar method for measuring water vapor profile in working PEMFC using WSP before [19]. However, the WSP method provides only the qualitative results and cannot quantitatively analyze water distribution. The quantitative HTP technique proposed in this study is upgraded beyond the previous qualitative WSP method. In this experiment, the current density distribution is also monitored using a segmented cell technique, and the effects of inlet humidification and flow configuration on the water transport and reaction distribution in the anode are investigated under low-humidity conditions. Finally, the paper provides the comparative discussion of water behaviors in two different flow configurations (co-flow and counter-flow).

2. Experimental

2.1. Humidity test paper (HTP)

To directly visualize water vapor distribution in the anode flow field of an operating PEMFC, humidity test paper (HTP), which is a test paper for water vapor detection manufactured by Advantec, is used in this experiment. Fig. 1 shows the discoloration images of HTP when exposed to six different humidity environments at 70 °C for 10 min. HTP is initially coated with a blue surface, and changed into red with an increase in water vapor concentration. Thereafter, when water concentration is decreased, the surface color is returned to the original blue. This discoloration process is reversible. Since it takes 5 min to complete the discoloration process of HTP, the HTP method cannot be applied to the fuel cell operation under unsteady state. In this experiment, the operation tests of fuel cell are conducted for a long time (1000 s) in constant-current mode, therefore they reach a steady state at the end of operations. The color images of HTP are captured by a CCD camera at $t = 1000$ s, after we confirmed that the HTP didn't discolor for 5 min. The thickness of HTP in the assembled cell is approximately 146 μm. The color image of HTP captured by a CCD camera can be quantitatively converted to the water vapor concentration based on the image processing. Fig. 2 presents the calibration curve between the R-component value in RGB color image of HTP and relative humidity at 70 °C.

2.2. Transparent fuel cell

Fig. 3 shows the schematic diagram of the transparent fuel cell used in this study. A PEM (Nafion-115) is sandwiched between two hydrophobic GDLs (Toray, TGP-H-060) in which Pt/C catalyst (Pt: 0.5 mg cm^{-2}) is loaded. The ionomer/carbon weight ratio (I/C) in the catalyst layer is adjusted to 1.0. The five-layer membrane electrode assembly (MEA) constructed of the PEM, two catalyst layers and two GDLs is sandwiched between two copper current collectors with gold coating. The anode-side current collector is divided into 10 segments to measure the current distribution as shown in Fig. 3(b). Each segment is connected with a separate current line. The active electrode area of the experimental cell is 5.0 cm^2. Two stainless steel separators, which have a single serpentine flow channel, are placed outside the current collectors. These separators are held together by four M6 bolts and tightened with a controlled torque of 0.3 Nm per bolt. The width, depth and length of the serpentine channel are 2.0 mm, 3.0 mm and 10.5 cm, respectively. To prevent gas leakage, the cell is sealed using silicone gaskets on each side of the MEA. For the visualization of water vapor distribution in the anode channel, three sheets of HTP (1.0 mm × 30 mm) are inserted between the anode GDL and current collector. The insertion of the HTP has a significant impact on

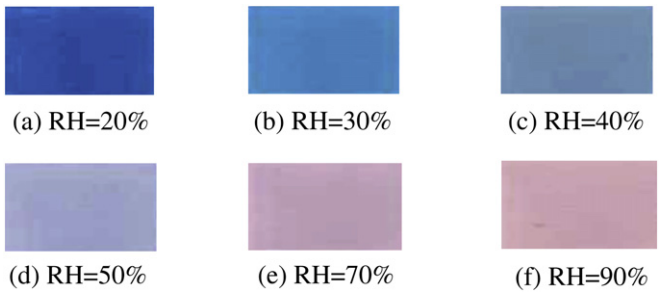

Fig. 1. Discoloration images of HTP when exposed to six different humidity environments for 10 min: (a) 20%, (b) 30%, (c) 40%, (d) 50%, (e) 70%, and (f) 90% RH.

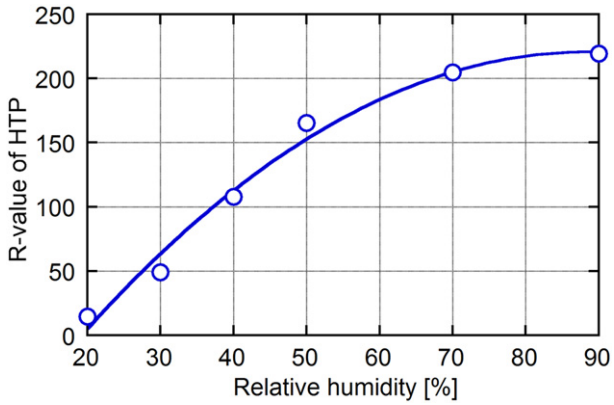

Fig. 2. Calibration curve between R-component value of HTP color image and relative humidity at 70 °C.

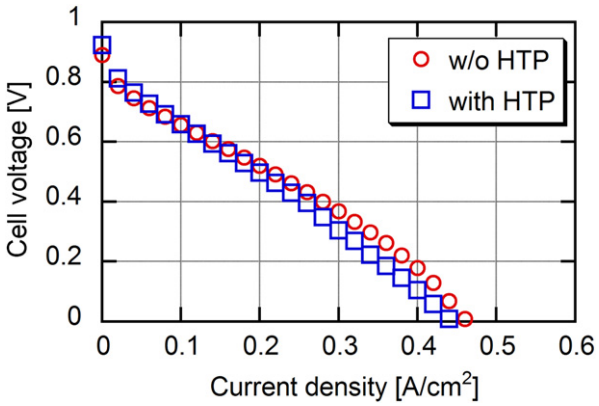

Fig. 4. Comparison of the polarization curves for two cases with and without HTP. The fuel cell was operated with dry H_2/O_2 at room temperature.

the cell performance. Fig. 4 provides the comparison of the polarization curves for two cases with and without HTP. The measurement of current–voltage (I–V) characteristics was conducted after the steady-state operation at room temperature. The anode and cathode gases are dry H_2 and O_2, respectively. As shown in the figure, the HTP insertion slightly reduces the cell voltage due to the contact resistance at the interface between the anode GDL and current collector. An increase in contact resistance due to the HTP installation is approximately 200 mΩ cm^2. To directly observe the discoloration of HTP in the anode flow field using a CCD camera, a transparent window is inserted into the anode separator.

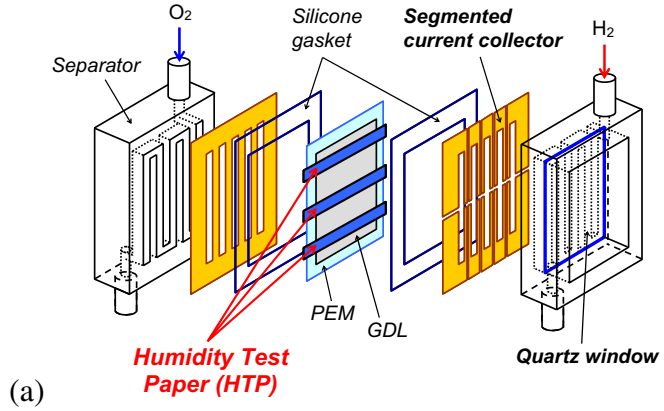

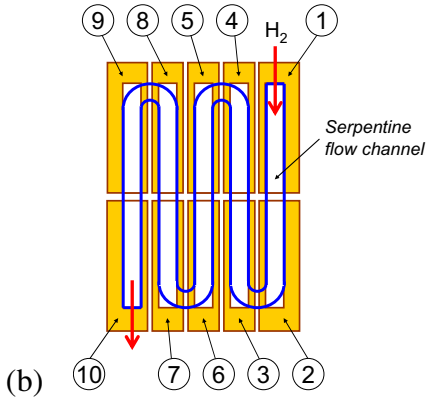

Fig. 3. Schematic diagram of the transparent fuel cell ((a) cell structure and (b) arrangement of the segmented current collector).

2.3. Experimental setup

Fig. 5 shows the experimental setup, which consists of a constant temperature chamber (Espec, LU-113), a gas supply unit, a digital CCD camera (Nikon, Micro-Nikkor lens (105 mm, f/2.8)), a transparent fuel cell, an electronic load (Kikusui, PLZ-164WA), a data logger (Hioki, 8420-50), and a personal computer. The transparent fuel cell equipped with a quartz window is operated in the constant temperature chamber in order to maintain the cell temperature. The CCD camera coupled with the zoom lens for the optical visualization is set outside of the constant temperature chamber, and the working distance (approximately 170 mm) from the anode channel of the transparent cell is adjusted. The anode flow field is illuminated by a halogen light source and the close-up images of the GDL surface can be clearly captured. The time-series output voltage of the operating fuel cell is recorded by the data logger. The high frequency resistance (HFR) of the PEM is measured by the LCR meter (Hioki, 3522-50).

The operating temperature and pressure of the experimental fuel cell are 70 °C and 1 atm. Pure hydrogen and oxygen as the fuel and oxidant are fed into the anode and cathode channels in the co-flow or counter-flow arrangement. The stoichiometries of H_2 and O_2 are fixed to be 2.5 and 5.0, respectively. The average current density is set to 0.3 A cm^{-2}. To investigate the influence of inlet gas humidification of the anode and cathode, three different combinations of anode/cathode = 30/0, 50/0, 0/30% RH are selected in this experiment.

2.4. Experimental procedure

The experimental procedure in this study is as follows:

(1) The pre-operation of the experimental fuel cell is carried out at 20 °C and 0.16 A cm^{-2} for 30 min to hydrate the electrolyte membrane. The HFR of the PEM is decreased to 650 mΩ cm^2, and the sufficient hydration of the membrane can be achieved in this step.
(2) After the pre-operation, the constant-current operation tests are performed at 70 °C under low-humidity conditions. During cell operation, the discoloration of HTP in the anode flow field is directly visualized by using the digital CCD camera. Furthermore, the current density distribution is measured using the segmented current collector. These two measurements are conducted separately in different experiments.
(3) After the operation test, the discoloration images of HTP captured by the CCD camera are quantitatively converted to the water vapor concentration based on the image post-processing.

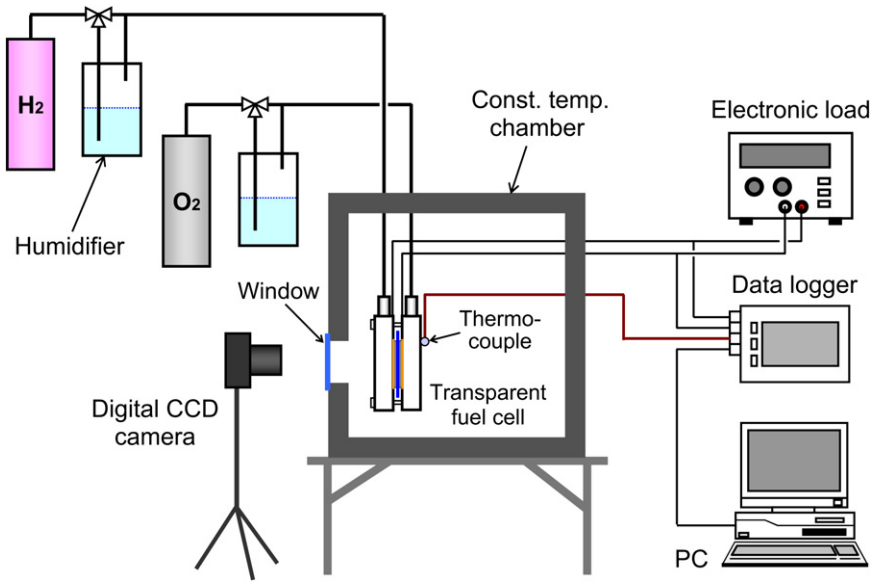

Fig. 5. Experimental setup.

3. Results and discussion

3.1. Effect of inlet gas humidification on water vapor and current distributions in anode of co-flow type PEMFC

Fig. 6 shows the discoloration images of HTP in the anode channel during cell operation, under three different anode and cathode inlet RH: A/C = 30/0, 50/0, 0/30%. Fig. 6(a) displays the original image of HTP before the operation test. The images of (b), (c) and (d) were captured at $t = 1000$ s after starting the operation. The anode gas (H_2) flows from the upper right to the lower left along the single serpentine channel in the co-flow mode. In the case of co-flow pattern, as shown in the photographic images of (b), (c) and (d), the HTP discolors to red remarkably in the downstream region. This indicates that the strong back-diffusion of product water from the cathode to anode occurs in the downstream and the water vapor concentration at the anode side rises strikingly. The high humidification of the anode inlet gas (A/C = 50/0% RH) vastly increases the water vapor concentration within the anode channel and improves the membrane hydration. Fig. 7 presents the distributions of relative humidity as a function of the fractional distance along the anode flow path of the co-flow cell for three test cases. These plots were analytically obtained from the color images of HTP shown in Fig. 6. To confirm the reproducibility of the experimental data, the measurements were repeated at least three times under the same conditions. The repeatability error of the water vapor measurement is within 3.5%. In the case of dry cathode inlet (A/C = 30/0, 50/0% RH), the profile of water vapor concentration along the anode channel first decreases near the inlet due to the electro-osmotic drag and forward-diffusion of water from the anode to

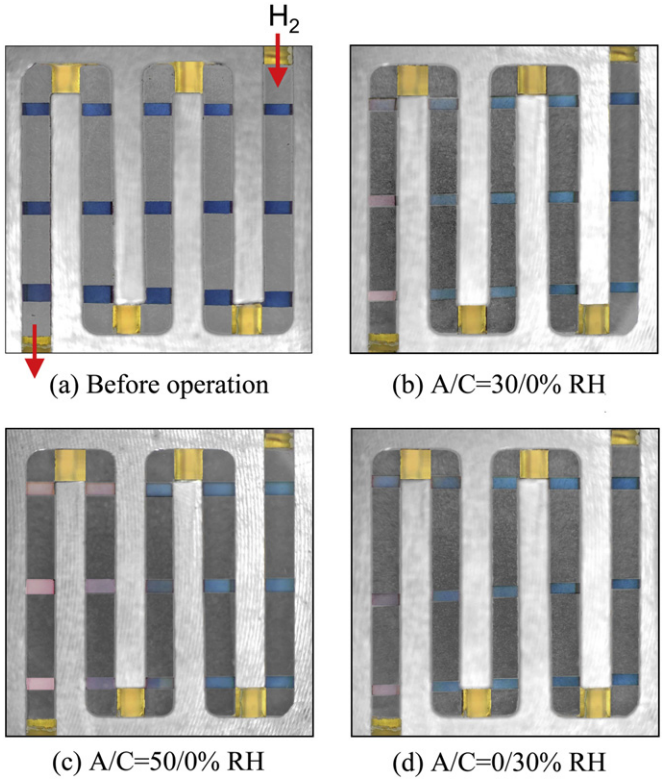

Fig. 6. Visualization images of HTP in the anode flow channel of the co-flow cell ((a) before operation, (b) A/C = 30/0% RH, (c) A/C = 50/0% RH, and (d) A/C = 0/30% RH).

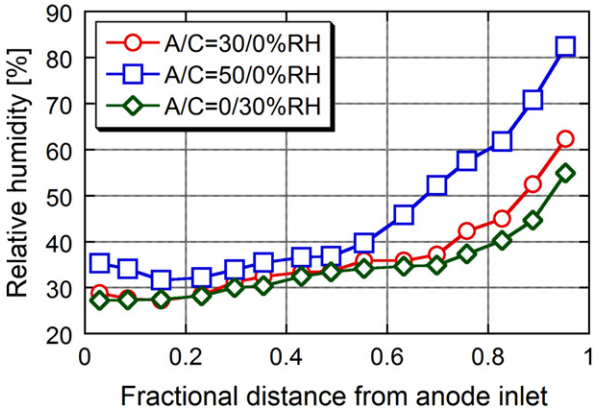

Fig. 7. Distributions of water vapor concentration along the anode flow path of the co-flow cell for three test cases: A/C = 30/0, 50/0, 0/30% RH.

cathode. After the minimum point, the water concentration increases toward the outlet, indicating that the strong back-diffusion of product water from the cathode exceeds the electro-osmotic drag. Even if only the anode inlet gas is partially humidified to 50% RH, the relative humidity at the anode exit reaches more than 80%. Needless to say, the increase of water vapor distribution in the anode is also partially affected by the hydrogen consumption along the flow channel. For the other case (A/C = 0/30% RH), the water vapor distribution in the anode channel increases monotonically due to the enhanced back-diffusion.

Fig. 8 shows the current density distributions along the anode flow path of the co-flow configuration under three humidification conditions of A/C = 30/0, 50/0, 0/30% RH. The locally resolved current density was measured with segmented cell structure concept after 1000 s of operation. Each plot was obtained by averaging three experimental data. The repeatability error of the current measurement is within 10%. It is noted that the current distributions increase almost linearly along the flow path in all cases. Since the membrane hydration is insufficient near the anode inlet for the co-flow configuration, the local current density is relatively low in the upstream region. In the cases of A/C = 30/0, 50/0% RH, the current density profiles have the bottom points near the inlet because of low water concentration on the anode side.

3.2. Water vapor and current distributions in anode of counter-flow type PEMFC

Water transport and reaction distribution in PEMFC during low-humidity operation are strongly influenced by flow configuration as well as inlet gas humidification of anode and cathode. Fig. 9 shows the visualization images of HTP in the anode channel of the counter-flow cell under three different anode and cathode inlet RH. Fig. 9(a) is the original image of HTP before the operation. The images of (b), (c) and (d) were captured after 1000 s of operation at A/C = 30/0% RH, A/C = 50/0% RH and A/C = 0/30% RH, respectively. The anode gas flows from the upper right to the lower left along the serpentine channel in the counter-flow mode. In the counter-flow configuration, the HTP on the anode side remarkably discolors to red in the midstream region. The water vapor concentration along the anode channel first increases near the anode inlet owing to the strong back-diffusion of water from the highly wetted cathode outlet. After the maximum point, the water concentration then decreases rapidly due to the forward-diffusion to the dry cathode inlet. The counter-flow arrangement improves the water management at the anode inlet region of the low-humidity PEMFC, and

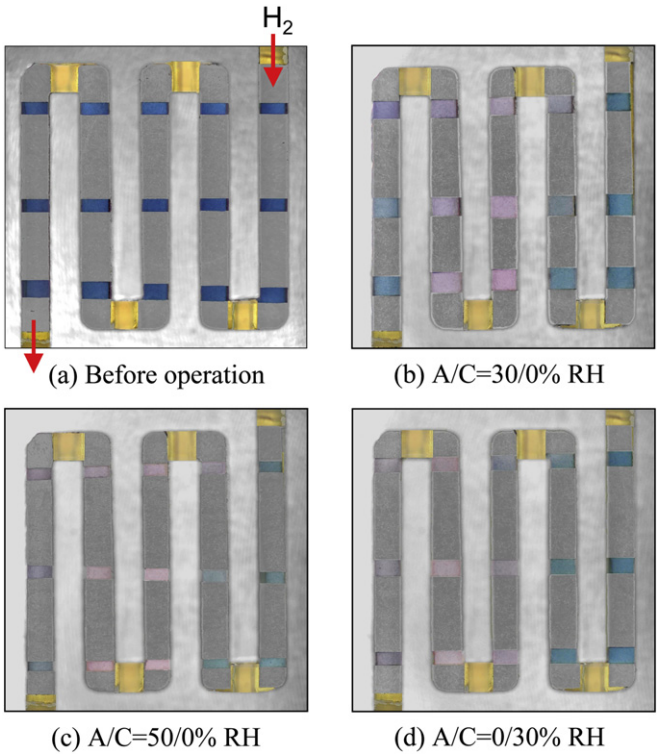

Fig. 9. Visualization images of HTP in the anode flow channel of the counter-flow cell ((a) before operation, (b) A/C = 30/0% RH, (c) A/C = 50/0% RH, and (d) A/C = 0/30% RH).

prevents the membrane dehydration. Fig. 10 presents the profiles of water vapor concentration along the anode flow path of the counter-flow cell for three humidification conditions. The color images of HTP provided in Fig. 9 were quantitatively converted to the relative humidity data. In all cases, the water vapor concentration along the anode channel increases remarkably in the anode upstream section, because the strong back-diffusion of water from the wetted cathode outlet greatly surpasses the electro-osmotic effect. However, only in the case of A/C = 50/0% RH, we observe a sudden drop of the relative humidity at the anode entrance, indicating that the electro-osmotic drag causes the water transport from the anode to cathode. The water vapor distributions have the maximum values at the fractional location of x/L = 0.5–0.6. In the downstream region of anode, although the hydrogen is considerably consumed by the electrochemical reaction, the water vapor

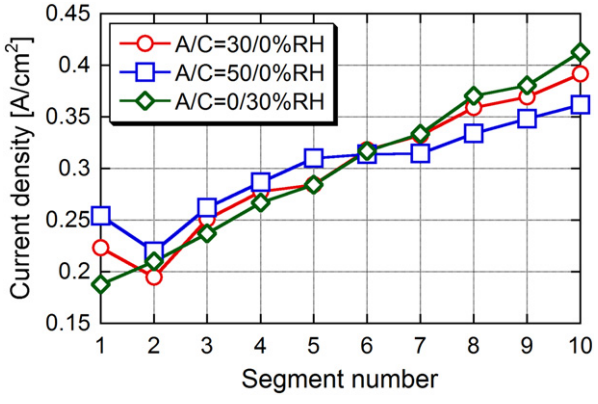

Fig. 8. Current density distributions along the anode flow path of the co-flow configuration under three humidification conditions: A/C = 30/0, 50/0, 0/30% RH.

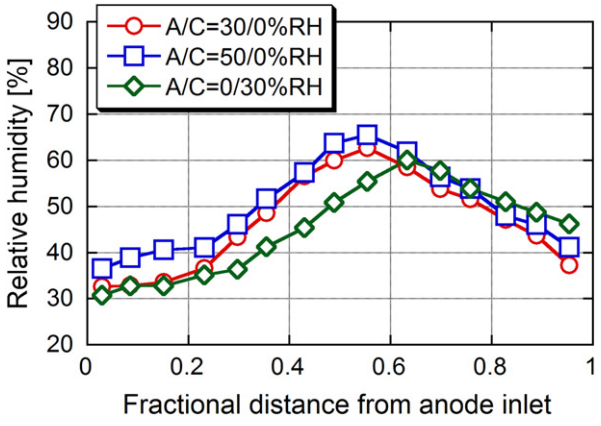

Fig. 10. Distributions of water vapor concentration along the anode flow path of the counter-flow cell for three test cases.

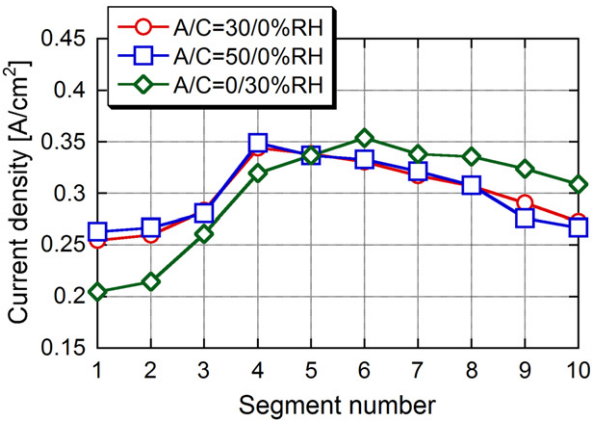

Fig. 11. Current density distributions along the anode flow path of the counter-flow configuration under three humidification conditions.

concentration reduces due to the forward-diffusion to the dry cathode inlet. The high humidification of the anode inlet (A/C = 50/0% RH) enhances the water concentration especially in the anode upstream region of the counter-flow cell. On the other hand, the cathode inlet humidification of A/C = 0/30% RH suppresses the water shortage at the anode outlet.

Fig. 11 shows the current density profiles along the anode flow path of the counter-flow cell for three cases. The current measurement was conducted at $t = 1000$ s after starting the operation. In the counter-flow mode, the maximum local current density can be observed in the midstream region because the water content in the electrolyte membrane is high. The anode inlet humidification improves the proton conductivity in the anode upstream region because of high water vapor concentration, and enhances the current density. In contrast, in the case of cathode inlet humidification (A/C = 0/30% RH), the local current density concentrates downstream in the anode flow field.

3.3. Comparison of cell performance

Fig. 12 provides the polarization curves of the co-flow cell under three different anode and cathode inlet RH. These *I–V* measurements were performed at $t = 1000$ s after the constant-current operation test. In the *I–V* and HFR measurements, the HTP was not inserted into the cell. It can be seen that the limiting current density in the case of A/C = 50/0% RH is higher as compared with those in the other two cases. The high humidification of anode inlet

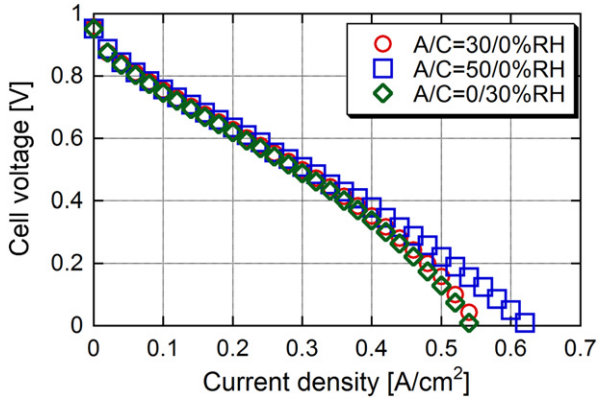

Fig. 12. Polarization curves of the co-flow cell under three different anode and cathode inlet RH: A/C = 30/0, 50/0, 0/30%.

Table 1
High frequency resistances (HFRs) of the electrolyte membrane for three humidification conditions.

	A/C = 30/0% RH	A/C = 50/0% RH	A/C = 0/30% RH
HFR (mΩ cm^2)	480	410	530

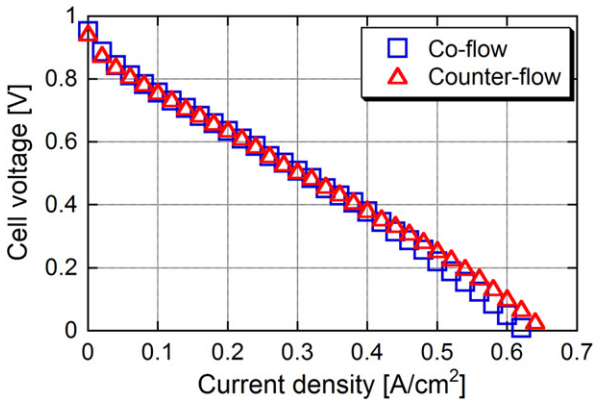

Fig. 13. Comparison of the polarization curves between the co-flow and counter-flow configurations at A/C = 50/0% RH.

gas improves the membrane hydration near the anode entrance, resulting in an increase in power density. The high frequency resistances (HFRs) of the electrolyte membrane for each case are described in Table 1. The membrane HFRs were measured based on AC impedance spectroscopy after the constant-current operation test. The measuring frequency of HFR is set to 100 kHz. It is found that the membrane HFR with humidifying the anode inlet becomes lower than that with humidifying the cathode inlet. During low-humidity operation, humidification of anode inlet gas effectively improves membrane hydration and enhances proton conductivity.

Fig. 13 shows the comparison of the polarization curves between the co-flow and counter-flow configurations at A/C = 50/0% RH. The limiting current density for the counter-flow cell is slightly higher than that for the co-flow cell because of the higher water content in the electrolyte membrane. Table 2 presents the membrane HFRs for both the co-flow and counter-flow type cells. The counter-flow arrangement promotes the membrane hydration especially near the anode inlet, leading to a decrease in PEM resistance.

Fig. 14 schematically illustrates the water transport processes between the anode and cathode in the co-flow and counter-flow type PEMFCs under dry cathode inlet conditions. In the co-flow configuration, the supplied water to the anode inlet immediately transfers toward the dry cathode near the inlet due to the electro-osmotic drag and forward diffusion. As a result, the water vapor concentration at the anode side seriously decreases in the upstream region, and a shortage of water for proton hydration and conduction arises in the electrolyte membrane. On the other hand, in the counter-flow cell, the strong back-diffusion of product water from the cathode to anode occurs near the anode inlet. Therefore, the anode inlet gas is immediately humidified by the back-diffused water from the cathode downstream region, and the sufficient

Table 2
Membrane HFRs for both the co-flow and counter-flow type cells operating at A/C = 50/0% RH.

	Co-flow	Counter-flow
HFR (mΩ cm^2)	410	370

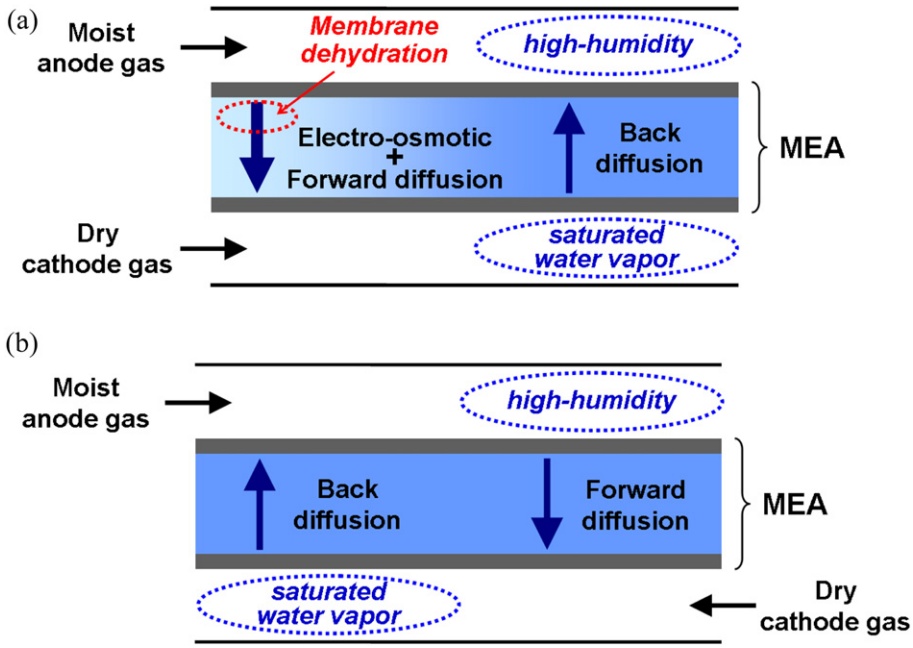

Fig. 14. Illustrations of the water transport between the anode and cathode in the (a) co-flow and (b) counter-flow type PEMFCs under dry cathode inlet conditions.

water content in the membrane can be achieved near the anode inlet. Counter-flow arrangement effectively improves water management in electrolyte membrane of PEMFC under low-humidity conditions.

4. Conclusions

To understand the water transport in a PEMFC under low-humidity operation, this paper presented a novel measurement technique for quantitatively estimating the water vapor distribution in the anode flow field using humidity test paper (HTP). In addition, the resolved local current was measured by a segmented cell approach, and the influences of inlet gas humidification and flow arrangement on the water behavior and reaction distribution inside the low-humidity PEMFC were discussed. In the conclusions, this paper mainly focused on the comparative evaluation of water transports in both co-flow and counter-flow cells. Especially, the following conclusions can be drawn from this study.

(1) In the co-flow configuration with the dry cathode inlet, the water vapor concentration along the anode flow path initially decreases near the inlet due to the electro-osmotic drag and forward-diffusion of water. Thereafter, the water concentration inversely increases toward the anode outlet because the strong back-diffusion of water from the cathode to anode arises in the downstream region. Co-flow arrangement in low-humidity PEMFC unfortunately causes insufficient membrane hydration and locally low current density near inlet area.
(2) The high humidification of the anode inlet gas enhances the water vapor concentration within the anode channel and prevents the membrane dehydration especially near the anode inlet.
(3) In the counter-flow cell, the water vapor concentration along the anode channel immediately increases in the upstream region due to the strong back-diffusion of water from the highly wetted cathode outlet. The distribution patterns of both water concentration and current density have a peak in the mid-stream section. Counter-flow configuration effectively improves water management and proton conductivity at anode inlet region during low-humidity operation.
(4) The performance comparison between the co-flow and counter-flow type PEMFCs was performed by measuring the polarization curve and membrane HFR. The limiting current density for the counter-flow cell is higher than that for the co-flow cell because of the superior membrane hydration. The counter-flow arrangement enhances the water content in the electrolyte membrane, resulting in a decrease in PEM resistance.

References

[1] R.J. Bellows, M.Y. Lin, M. Arif, A.K. Thompson, D. Jacobson, J. Electrochem. Soc. 146 (1999) 1099–1103.
[2] R. Satija, D.L. Jacobson, M. Arif, S.A. Werner, J. Power Sources 129 (2004) 238–245.
[3] D. Kramer, J. Zhang, R. Shimoi, E. Lehmann, A. Wokaun, K. Shinohara, G.G. Scherer, Electrochim. Acta 50 (2005) 2603–2614.
[4] J. Zhang, D. Kramer, R. Shimoi, Y. Ono, E. Lehmann, A. Wokaun, K. Shinohara, G.G. Scherer, Electrochim. Acta 51 (2006) 2715–2727.
[5] A. Turhan, K. Heller, J.S. Brenizer, M.M. Mench, J. Power Sources 160 (2006) 1195–1203.
[6] M.A. Hickner, N.P. Siegel, K.S. Chen, D.N. McBrayer, D.S. Hussey, D.L. Jacobson, M. Arif, J. Electrochem. Soc. 153 (2006) A902–A908.
[7] K. Yoshizawa, K. Ikezoe, Y. Tasaki, D. Kramer, E.H. Lehmann, G.G. Scherer, J. Electrochem. Soc. 155 (2008) B223–B227.
[8] P. Boillat, D. Kramer, B.C. Seyfang, G. Frei, E. Lehmann, G.G. Scherer, A. Wokaun, Y. Ichikawa, Y. Tasaki, K. Shinohara, Electrochem. Commun. 10 (2008) 546–550.
[9] T. Sasabe, S. Tsushima, S. Hirai, Int. J. Hydrogen Energy 35 (2010) 11119–11128.
[10] S.J. Lee, N.Y. Lim, S. Kim, G.G. Park, C.S. Kim, J. Power Sources 185 (2008) 867–870.
[11] P.K. Sinha, P. Halleck, C.Y. Wang, Electrochem. Solid-State Lett. 9 (2006) A344–A348.
[12] K. Tüber, D. Pócza, C. Hebling, J. Power Sources 124 (2003) 403–414.
[13] X.G. Yang, F.Y. Zhang, A.L. Lubawy, C.Y. Wang, Electrochem. Solid-State Lett. 7 (2004) A408–A411.
[14] F.Y. Zhang, X.G. Yang, C.Y. Wang, J. Electrochem. Soc. 153 (2006) A225–A232.
[15] S. Ge, C.Y. Wang, J. Electrochem. Soc. 154 (2007) B998–B1005.
[16] S. Litster, D. Sinton, N. Djilali, J. Power Sources 154 (2006) 95–105.
[17] K. Nishida, T. Murakami, S. Tsushima, S. Hirai, J. Power Sources 195 (2010) 3365–3373.
[18] S. Tsushima, K. Teranishi, S. Hirai, Electrochem. Solid-State Lett. 7 (2004) A269–A272.

[19] K. Nishida, M. Ishii, S. Tsushima, S. Hirai, J. Power Sources 199 (2012) 155–160.
[20] M.M. Mench, Q.L. Dong, C.Y. Wang, J. Power Sources 124 (2003) 90–98.
[21] Q. Dong, J. Kull, M.M. Mench, J. Power Sources 139 (2005) 106–114.
[22] Q. Dong, M.M. Mench, S. Cleghorn, U. Beuscher, J. Electrochem. Soc. 152 (2005) A2114–A2122.
[23] X.G. Yang, N. Burke, C.Y. Wang, K. Tajiri, K. Shinohara, J. Electrochem. Soc. 152 (2005) A759–A766.
[24] F. Liu, G. Lu, C.Y. Wang, J. Membr. Sci. 287 (2007) 126–131.
[25] G.Q. Lu, F.Q. Liu, C.Y. Wang, J. Power Sources 164 (2007) 134–140.
[26] Y. Fujii, S. Tsushima, K. Fukuzato, S. Hirai, ECS Trans. 16 (2008) 1635–1642.